ACCELEROMETER CALIBRATION USING SENSOR FUSION WITH A GYROSCOPE

Fredrik Olsson[a], *Manon Kok*[b], *Kjartan Halvorsen*[a,c], *Thomas B. Schön*[a]

[a]Department of Information Technology, Uppsala University, Uppsala, Sweden
[b]Department of Electrical Engineering, Linköping University, Linköping, Sweden
[c]Department of Mechatronics, Instituto Tecnologico y de Estudias Superiores de Monterrey, Atizapan, Mexico

ABSTRACT

In this paper, a calibration method for a triaxial accelerometer using a triaxial gyroscope is presented. The method uses a sensor fusion approach, combining the information from the accelerometers and gyroscopes to find an optimal calibration using Maximum likelihood. The method has been tested by using real sensors in smartphones to perform orientation estimation and verified through Monte Carlo simulations. In both cases, the method is shown to provide a proper calibration, reducing the effect of sensor errors and improving orientation estimates.

***Index Terms*—** Calibration, MEMS, Accelerometer, Sensor fusion, Maximum likelihood.

1. INTRODUCTION

Accelerometers and gyroscopes (inertial sensors) measure linear acceleration and angular velocity, respectively. By combining three orthogonal accelerometers and three orthogonal gyroscopes, it is possible to measure in three dimensions. These types of sensors have many different applications, for example in navigation and motion capture [1]. Advances in micro-electromechanical systems (MEMS) have made inertial sensors widely available in everyday life, for instance in smartphones. MEMS sensors are relatively small, cheap and have low power consumption. The accuracy of these sensors is highly dependent on a proper calibration that removes systematic errors and sensor biases. Calibration refers to the procedure of measuring some known quantity and estimating sensor parameters such that the measurement output agree with that known information. An example of the type of calibration discussed in this paper can be seen in Fig. 1. MEMS inertial sensors are only approximately calibrated by the manufacturer, and some sensor errors change over time [2]. Therefore, in order to obtain high accuracy measurements, the sensors have to be recalibrated in the field.

Most existing methods for accelerometer calibration use measurements from a set of different static orientations to estimate a set of parameters. These methods are based on the fact that the magnitude of the measured acceleration should be equal to the local gravitational acceleration in static conditions. The choice of calibration method largely depends on the existing systematic errors. Some methods estimate three gains and three bias parameters [3, 4]. This is sufficient if the accelerometer axes can be assumed to be perfectly orthogonal, and if the cross-axis interference caused by electric coupling in the electronics is negligible [5]. For lower quality sensors these assumptions are typically not valid, and as a result of this, up to three additional parameters have to be introduced and estimated to compensate for these errors [6].

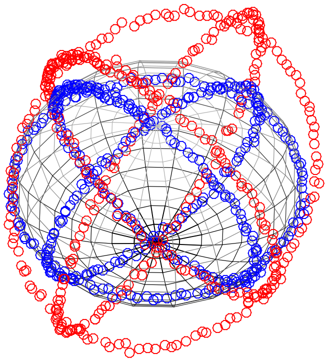

Fig. 1: Illustration of synthetic calibrated and uncalibrated accelerometer measurements in 3D. The calibrated measurements $\mathbf{y}_t^{\text{cal}}$ (blue) are centered on a sphere with radius $\|\mathbf{g}\|_2$ centered around the origin. The uncalibrated measurements $\mathbf{y}_t$ (red) form an ellipsoid, possibly centered around an offset.

The methods discussed above concern the calibration of a standalone triaxial accelerometer. However, if there are more sensors available in the same platform, it makes sense to use a sensor fusion approach. More specifically, accelerometers are typically available in combination with gyroscopes. Using these sensors together, it is possible to formulate the calibration problem as a problem of estimating the sensor's orientation in the presence of unknown calibration parameters. A similar approach is used by Kok and Schön in [7] for magnetometer calibration. They assume, however, that the accelerometers are calibrated, which may not always hold for lower quality sensors.

When calibrating sensors which are mounted in a larger sensor platform, the relative orientation between the sensors becomes of interest. To compensate for this inter-sensor misalignment, three additional parameters need to be estimated [8, 9], giving a total of 12 calibration parameters.

In this paper we present a calibration method for a triaxial accelerometer using a sensor fusion approach similar to [7]. However, we only use information from the inertial sensors and disregard the magnetometer. Including the gyroscope measurements allows for more freedom in the way the sensors are rotated during the calibra-

This work was supported by the project *Mobile assessment of human balance* (Contract number: 2015-05054), and by CADICS, a Linnaeus Center, both funded by the Swedish Research Council.

High accuracy reference measurements are provided through the use of the Vicon real-time tracking system courtesy of the UAS Technologies Lab, Artificial Intelligence and Integrated Computer Systems Division (AIICS) at the Department of Computer and Information Science (IDA), Linköping University, Sweden. http://www.ida.liu.se/divisions/aiics/aiicssite/index.en.shtml

tion procedure. The goal of this method is to allow for lower quality sensors to be used in applications which require measurements of a higher accuracy than these sensors initially provide.

2. MODEL AND PROBLEM FORMULATION

To formulate the calibration problem for the accelerometer we first need to model the rotation of the sensor platform. Using the angular velocity measurements provided by the gyroscope, we formulate a dynamic model, which uses the gyroscope measurements as inputs to predict the orientation of the sensor

$$\mathbf{x}_{t+1} = \mathbf{x}_t \odot \mathbf{exp}\frac{\Delta_t}{2}\omega_t, \tag{1}$$

where the state variables $\mathbf{x}_t$ are unit quaternions, $\odot$ denotes the quaternion multiplication and $\mathbf{exp}$ the vector exponential. For background on quaternion algebra, see e.g. [10]. The input to the dynamic model is the angular velocity ω_t, at time t, sampled with interval Δ_t. The gyroscope measurements, $\bar{\omega}_t$, are modelled as

$$\bar{\omega}_t = \omega_t + \mathbf{b}_\omega + \mathbf{v}_t, \tag{2}$$

where $\mathbf{b}_\omega$ is the gyroscope bias and $\mathbf{v}_t \sim \mathcal{N}(0, \Sigma_\omega)$ is Gaussian measurement noise. Estimating and removing the bias $\mathbf{b}_\omega$ from (2) will allow us to use the gyroscope measurements as input to (1).

Next we model the accelerometer measurements, which depend on the orientation of the sensor platform and the unknown calibration parameters to be estimated. The raw (uncalibrated) accelerometer measurements, $\mathbf{y}_t$, are modelled as

$$\mathbf{y}_t = \mathbf{D}\mathbf{R}(\mathbf{x}_t)\mathbf{g} + \mathbf{b}_a + \mathbf{e}_t, \tag{3}$$

where $\mathbf{R}(\mathbf{x}_t)$ is a rotation matrix describing the orientation of the sensor. The sensor is assumed to be in constant linear velocity in the gravitational field with acceleration $\mathbf{g}$, which is true for stationary sensors. The local gravitational acceleration $\mathbf{g}$ is also assumed to be known. The sensor bias is modelled by the vector $\mathbf{b}_a \in \mathbb{R}^{3\times1}$ and $\mathbf{e}_t \sim \mathcal{N}(0, \Sigma_a)$ is Gaussian measurement noise. Gains, non-orthogonal sensor axes, cross-axis interference and inter-sensor misalignments are modelled by the matrix $\mathbf{D} \in \mathbb{R}^{3\times3}$. In fact, $\mathbf{D}$ can be seen as a product of matrices that model these errors separately, and the number of unknown parameters that make up the elements of $\mathbf{D}$ can be reduced if some of these errors are ignored. The desired error-free accelerometer output is $\mathbf{R}(\mathbf{x}_t)\mathbf{g}$. Therefore, if $\mathbf{D}$ and $\mathbf{b}_a$ are known, the calibrated accelerometer measurements can be calculated as

$$\mathbf{y}_t^{\text{cal}} = \mathbf{D}^{-1}(\mathbf{y}_t - \mathbf{b}_a). \tag{4}$$

In 3D space the calibrated accelerometer measurements will form a sphere of radius $\|\mathbf{g}\|_2$ with its center in the origin, while the uncalibrated measurements form an ellipsoid centered around the sensor bias $\mathbf{b}_a$, see Fig. 1.

The calibration problem is formulated as a Maximum likelihood (ML) estimation problem for the unknown model parameters $\theta = \{\mathbf{D}, \mathbf{b}_a\}$, where the ML estimator for θ is given by

$$\widehat{\theta} = \arg\max_\theta p_\theta(\mathbf{y}_{1:T}) = \arg\max_\theta \prod_{t=1}^{T} p_\theta(\mathbf{y}_t|\mathbf{y}_{1:t-1}), \tag{5}$$

using all measurements from time $t = 1$ to T, and the convention that $\mathbf{y}_{1:0} = \emptyset$. The likelihood function, $p_\theta(\mathbf{y}_{1:T})$, is obtained from the one step ahead predictors, $p_\theta(\mathbf{y}_t|\mathbf{y}_{1:t-1})$. We use an extended Kalman filter (EKF) to approximate the one step ahead predictors. The EKF uses the nonlinear state space model given by (1) and (3), and estimates the orientation of the sensor platform as the unit quaternion states $\mathbf{x}_t$. For more details about the EKF implementation, see e.g. [11]. The one step ahead predictors are then approximated as

$$p_\theta(\mathbf{y}_t|\mathbf{y}_{1:t-1}) \approx \mathcal{N}(\mathbf{y}_t|\widehat{\mathbf{y}}_{t|t-1}(\theta), \mathbf{S}_t(\theta)), \tag{6}$$

which is a probability density function of a Gaussian random variable $\mathbf{y}_t$ with mean $\widehat{\mathbf{y}}_{t|t-1}(\theta)$ and covariance matrix $\mathbf{S}_t(\theta)$.

An equivalent formulation of (5) is

$$\widehat{\theta} = \arg\min_\theta V(\theta), \tag{7}$$

where $V(\theta)$ is the negative log-likelihood, which will be referred to as the cost function. It is given by

$$V(\theta) = \frac{1}{2}\sum_{t=1}^{T} \|\mathbf{y}_t - \widehat{\mathbf{y}}_{t|t-1}(\theta)\|^2_{\mathbf{S}_t^{-1}(\theta)} + \log\det\mathbf{S}_t(\theta), \tag{8}$$

where $\|\cdot\|_{\mathbf{S}_t^{-1}(\theta)}$ is the 2-norm weighted by the inverse of the covariance matrix. From the Kalman filter theory we can recognize $\mathbf{y}_t - \widehat{\mathbf{y}}_{t|t-1}(\theta)$ as the output innovations, and $\mathbf{S}_t(\theta)$ as the innovation covariance. The EKF is hence used to evaluate the cost function (8), which allows the optimization problem (7) to be solved using an iterative method, see Section 3.

3. CALIBRATION ALGORITHM

The calibration algorithm, summarized in Algorithm 1, works on sets of sequential measurements that should be divided into two subsequent segments. In the first segment, the sensors are stationary on a flat surface and in the second segment the sensors are rotated into different orientations. The first segment is used to estimate the initial orientation, $\mathbf{x}_0$, of the sensors and to estimate the parameters $\mathbf{b}_\omega, \Sigma_a$ and Σ_ω. The noise covariance matrices Σ_a and Σ_ω are assumed to be diagonal. The gyroscope is assumed to be calibrated after this first part. The second segment is then used to solve the optimization problem in (7) for the parameters θ, with an iterative method. In every iteration, the cost function (8) is evaluated by running the orientation estimation EKF described in Section 2, using the current parameter estimates. To solve the optimization problem (7) we use a Gauss-Newton method [12], which requires the gradients and the approximate Hessian of the cost function. However, computing the gradients of (8) is not straightforward, since the predicted state $\hat{\mathbf{x}}_{t|t-1}$ depends on the parameters θ through the previous measurement updates of the filter. Therefore, a numerical gradient of the cost function is calculated by approximating the partial derivatives $\frac{dV(\theta)}{d\theta}$ using finite differences. The numerical gradient is then used to approximate the Hessian as $(\frac{dV(\theta)}{d\theta})^T(\frac{dV(\theta)}{d\theta})$. Two independent stopping criteria are used for the optimization algorithm. The first criterion requires the Newton decrement [13] to be smaller than some constant ϵ_1. The second criterion will stop the algorithm if the calculated step length found in the line search is smaller than some other constant ϵ_2, and does not satisfy the Wolfe conditions [12]. The constants ϵ_1 and ϵ_2 can be chosen as a compromise between accuracy and computation speed.

4. EXPERIMENTAL RESULTS

The calibration algorithm was tested in two separate experiments using real sensors in two different smartphones (Samsung

Algorithm 1 Calibration algorithm

```
1: Estimate accelerometer and gyroscope covariance, gyroscope bias and the initial orientation of the sensor, $\widehat{\Sigma}_a, \widehat{\Sigma}_\omega, \widehat{\mathbf{b}}_\omega, \widehat{\mathbf{x}}_0$ from a stationary portion of the sampled measurements.
2: Initialize $\widehat{\mathbf{D}}_0 = \mathbf{I}_3$, a $3 \times 3$ identity matrix and $\mathbf{b}_{a,0} = \mathbf{0}_{3\times 1}$, a $3 \times 1$ zero vector.
3: Set $i = 0$ and repeat:
4: Run the EKF using the current estimates $\widehat{\theta}_i = \{\widehat{\mathbf{D}}_i, \widehat{\mathbf{b}}_{a,i}\}$ and the initial orientation $\widehat{\mathbf{x}}_0$.
5: Approximate the partial derivatives of the cost function (8) as finite differences and calculate the approximate Hessian.
6: Calculate $\widehat{\theta}_{i+1}$ by solving (7) as an unconstrained optimization problem using a Gauss-Newton method and a line search algorithm [12].
7: Set $i = i + 1$ and repeat from step 4 until convergence.
```

Galaxy S5 and Google Nexus 4). Specifically, the sensors used were the MPU-6050 for the Google Nexus 4, and the MPU-6500 for the Samsung Galaxy S5, both sensors are manufactured by InvenSense [14]. These sensors were of interest as we have previously seen distinct variations in the magnitudes of the accelerometer measurements for different orientations in stationary conditions, when using these sensors. The method was also verified using synthetic data.

4.1. Real sensor data

In the first experiment, sensor data was collected from a Samsung Galaxy S5 smartphone. The smartphone was initially at rest on a flat surface for approximately 10 seconds. Subsequently, the phone was picked up and rotated by hand. Two different datasets were collected using different types of rotation. For the first dataset, the smartphone was rotated into 6 different pre-specified orientations, separated by approximately 90 degrees. The smartphone was stationary in these orientations for periods of approximately 10 seconds before it was rotated again. For the second dataset, the smartphone was continuously rotated around all of its axes. The datasets were used to calibrate the sensors in the phone using Algorithm 1.

The results for the two datasets are seen in Fig. 2. After calibrating the accelerometer the measurement magnitudes become centered, close to $\|\mathbf{g}\|_2 = 9.82\mathrm{m\,s^{-2}}$. The average magnitude of the calibrated data was $9.81(\sigma = 0.23)\mathrm{m\,s^{-2}}$ for the first dataset, and $9.80(\sigma = 0.30)\mathrm{m\,s^{-2}}$ for the second dataset, with standard deviations σ. This is a significant improvement over the uncalibrated measurements, where the magnitude varies for different orientations.

Every time the phone is rotated the accelerometer data violates the measurement model, which assumes that the accelerometer is only affected by the gravitational acceleration. The second dataset therefore contains more outliers than the first dataset. The effect of having outliers in the calibration data is not examined further in this paper. However, it could result in improper calibrations if the number of outliers becomes very large.

4.2. Orientation estimation

In the second experiment a Google Nexus 4 smartphone was used to test the calibration performance. The phone was attached to a board which was stationary at first, followed by one complete rotation around the roll, pitch and yaw axes. The rotation speed was in the order of $9°\mathrm{s^{-1}}$. This was repeated three times. Reflective markers, that were detected and tracked by an optical reference system (Vicon), were attached to the board. Using multiple markers, the orientation of the board was obtained with high accuracy and used as a reference. The measurements collected from the accelerometers and gyroscopes of the phone were used to estimate the orientation of the board using an EKF. The estimated orientations were then compared with the reference measurements. Data from the first stationary part and one rotation segment was used to calibrate the sensors, while the orientation estimation was performed on the whole dataset.

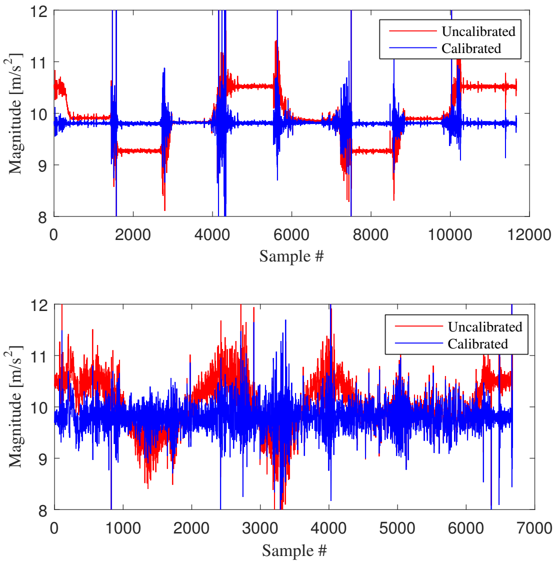

Fig. 2: Measurement magnitudes of the calibrated and uncalibrated accelerometer in the Samsung Galaxy S5, from the two datasets explained in Section 4.1. Top: The phone was rotated into 6 different fixed orientations. Bottom: The phone was continuously rotated by hand.

The orientations of interest here are the roll and pitch angles, which are observable by the accelerometer. The yaw angle, or heading, can only be observed by introducing additional sensors, for example a magnetometer. When using the uncalibrated accelerometer the average absolute error of the estimated roll and pitch angles was $3.43°$ and $1.61°$, respectively. The errors were reduced to $1.82°$ and $0.78°$, respectively, when using the calibrated accelerometer measurements.

4.3. Synthetic data

Monte Carlo simulations were performed to verify the functionality of the calibration algorithm. Sensors with randomly generated parameters were calibrated using synthetic data. The synthetic accelerometers had a gain in the range $(0.5, 1.5)$, a intersensor misalignment in the range of $\pm 10°$, non-orthogonal sensor axes in the range of $\pm 30°$ and a bias in the range of $\pm 1\mathrm{m\,s^{-2}}$. The synthetic gyroscopes had biases in the range of $\pm 1\mathrm{rad\,s^{-1}}$. The diagonal elements of the noise covariance matrices were in the range of $(10^{-3}, 10^{-1})$ and $(10^{-3}, 10^{-2})$ for the synthetic accelerometers and gyroscopes, respectively. All of the mentioned ranges have a uniform distribution. The synthetic data represented one complete rotation around each axis. A total of 1000 simulations were performed.

The difference between the calibrated and uncalibrated mea-

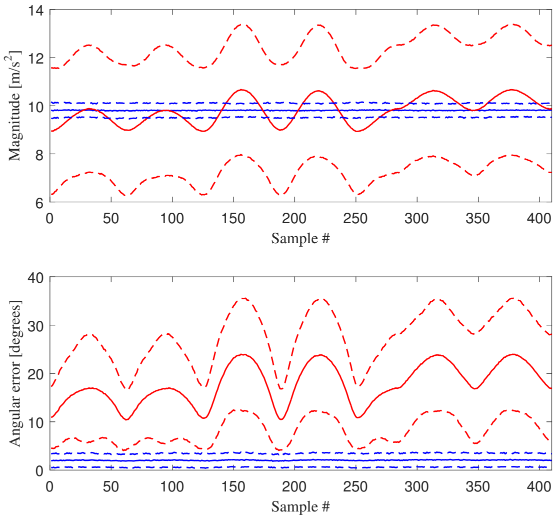

Fig. 3: Calibrated and uncalibrated measurement magnitudes and angular errors for 1000 Monte Carlo simulations. The blue lines represent the calibrated measurements $\mathbf{y}_t^{\text{cal}}$, and the red lines represent the uncalibrated measurements $\mathbf{y}_t$. The means are represented as solid lines with a confidence interval of one standard deviation, represented by the dashed lines.

surements can be seen in Fig. 3. After calibration, the magnitude of the measurements are significantly closer to the true magnitude $\|\mathbf{g}\|_2 = 9.82\mathrm{m\,s}^{-2}$. The absolute value of the angle between the calibrated measurement vectors $\mathbf{y}_t^{\text{cal}}$, and the ideal (noise- and error free) measurement vectors (the angular error), also decreased to an average of 2 degrees. The average absolute orientation estimation errors also decreased significantly from $8.3(\sigma = 7.1)^\circ$ to $0.32(\sigma = 0.40)^\circ$ for the roll angle, and from $8.3(\sigma = 6.9)^\circ$ to $0.33(\sigma = 0.43)^\circ$ for the pitch angle. To speed up these simulations, the Gauss-Newton method was allowed to perform a maximum of 10 iterations. However, the algorithm converged in 6 iterations or less on average.

4.4. Cramér-Rao lower bound

A common tool used to evaluate the performance of estimators is the Cramér-Rao lower bound (CRLB), which gives a lower bound on the variance of an unbiased estimator [15]. The CRLB was calculated using the mean Hessian from 100 simulations using one fixed set of parameters. The square root of the CRLB can be compared with the root-mean-square error (RMSE), for the estimated parameters $\widehat{\theta}$, see Fig. 4. The RMSE values were found to be close to the square root of the estimated CRLB which suggests that the estimator is efficient. Interestingly, for parameter 6, it can be seen that $\sqrt{\text{CRLB}} > \text{RMSE}$. This could be because of the numerical approximation of the CRLB or because there is a small bias in the parameter estimates.

5. CONCLUSIONS

In this paper, a calibration method for a triaxial accelerometer, using sensor fusion with a triaxial gyroscope in the same platform, has been presented. The main goal of the method is to allow sensor platforms with lower quality sensors, e.g. smartphones, to be used in applications which require higher accuracy measurements. The method has been tested using both real and synthetic data, and has been shown to accurately calibrate the sensors. The estimated parameters can be used to compensate for gain, inter-sensor misalignment, non-orthogonal sensor axes, cross-axis interference and bias. The method was used to calibrate the accelerometer in a smartphone, which brought the measurement magnitudes closer to $\|\mathbf{g}\|_2$. This was a significant improvement compared to the uncalibrated accelerometer, where the magnitudes varied for different orientations. It was also shown that the calibration works when using a smartphone to perform orientation estimation, improving the accuracy in the estimated roll and pitch angles. Monte Carlo simulations show a significantly reduced effect of sensor errors in the calibrated measurements. Simulations also showed that the RMSE was close to the $\sqrt{\text{CRLB}}$ for the estimated parameters, which suggests that the Maximum likelihood estimator is efficient. The Gaussian noise model used here cannot describe measurement outliers.

We see a number of interesting improvements and extensions of the method. The problem of too many outliers could be handled by different approaches: outlier detection, by using a heavytailed noise distribution or by using robust Kalman filtering [16]. Another possible future extension would be to combine the method with magnetometer calibration for more accurate heading estimates. In addition to these improvements, further analysis with sensors of varying quality, and comparisons to other methods would be interesting as future work.

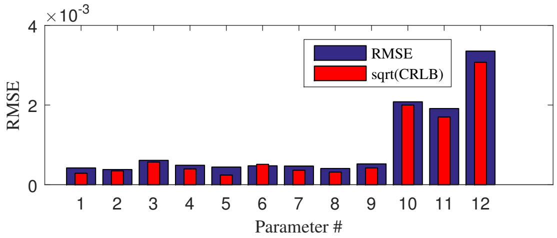

Fig. 4: Square root of the estimated CRLB and the RMSE for the estimated parameters for 100 simulations using the same set of parameters. The first 9 parameters belong to the vectorized matrix $\mathbf{D}$ and parameters 10-12 belong to the bias vector $\mathbf{b}_a$.

6. REFERENCES

[1] D. E. Serrano and F. Ayazi, *Resonant MEMS: Fundamentals, Implementation, and Application*, chapter MEMS Inertial Sensors, pp. 329–352, Wiley-VCH, 2015.

[2] O. J. Woodman, “An introduction to inertial navigation,” Tech. Rep. 696, University of Cambridge Computer Laboratory, August 2007.

[3] S. P. Won and F. Golnaraghi, “A triaxial accelerometer calibration method using a mathematical model,” *IEEE Transactions on Instrumentation and Measurement*, vol. 59, no. 8, pp. 2144 –2153, August 2010.

[4] N. Grip and N. Sabourova, “Simple non-iterative calibration for triaxial accelerometers,” *Measurement Science and Technology*, vol. 22, no. 12, pp. 125103, 2011.

[5] I. Frosio, F. Pedersini, and N. A. Borghese, “Autocalibration of triaxial MEMS accelerometer with automatic sensor model selection,” *IEEE Sensors Journal*, vol. 12, no. 6, pp. 2100–2108, June 2012.

[6] T. Forsberg, N. Grip, and N. Sabourova, “Non-iterative calibration for accelerometers with three non-orthogonal axes, reliable measurement setups and simple supplementary equipment,” *Measurement Science and Technology*, vol. 24, no. 3, pp. 035002, 2013.

[7] M. Kok and T. B. Schön, “Maximum likelihood calibration of a magnetometer using inertial sensors,” in *Proceedings of the 19th World Congress of the International Federation of Automatic Control (IFAC)*, Cape Town, South Africa, August 2014, pp. 92–97.

[8] G. Panahandeh, I. Skog, and M. Jansson, “Calibration of the accelerometer triad of an inertial measurement unit, maximum likelihood estimation and Cramér-Rao bound,” in *Procceedings of the International Conference on Indoor Positioning and Indoor Navigation (IPIN)*, Zurich, Switzerland, September 2010, pp. 1–6.

[9] B. Fang, W. Chou, and L. Ding, “An optimal calibration method for a MEMS inertial measurement unit,” *International Journal of Advanced Robotic Systems*, vol. 11, pp. 1–14, 2014.

[10] S. Särkkä, “Notes on quaternions,” Tech. Rep., 2007.

[11] M. Kok, “Probabilistic modeling for positioning applications using inertial sensors,” Licentiate’s thesis, Linköping University, Sweden, 2014.

[12] J. Nocedal and S. J. Wright, *Numerical Optimization*, Springer Series in Operations Research, 2nd edition, 2006.

[13] S. Boyd and L. Vandenberghe, *Convex Optimization*, Cambridge University Press, 2004.

[14] InvenSense, “6 Axis MotionTracking,” [Online] http://www.invensense.com/products/motion-tracking/6-axis/, May 2016.

[15] F. Gustafsson, *Statistical Sensor Fusion*, Studentlitteratur, 2012.

[16] J. Mattingley and S. Boyd, “Real-time convex optimization in signal processing,” *IEEE Signal Processing Magazine*, vol. 27, no. 3, pp. 50–61, May 2010.